JOC Article

Magnetic Interaction of Pyridyl-Substituted Thioaminyl Stable Free Radicals[1]

Yozo Miura,*,† Yuichi Oyama,† and Yoshio Teki*,‡

Department of Applied Chemistry, Graduate School of Engineering, and Department of Material Science and Chemistry, Graduate School of Science, Osaka City University, Sumiyoshi-ku, Osaka 558-8585, Japan

miura@a-chem.eng.osaka-cu.ac.jp

Received August 26, 2002

N-(2-Pyridylthio)-2,6-diaryl-4-R-phenylaminyls (R = Ph, 4-ClC_6H_4, MeCO, CN, EtOCO) and *N*-(4-pyridylthio)-2,6-diaryl-4-R-phenylaminyls (R = Ph, 4-ClC_6H_4, EtOCO) were prepared and isolated as radical crystals. Their ESR spectra were measured, and the NS and pyridyl nitrogen and anilino meta and pyridyl ortho and para proton hyperfine coupling constants were determined. The spin-density calculations based on the density functional theory were performed by the UBecke 3LYP hybrid method using the STO 6-31G basis set. X-ray crystallographic analyses were performed for three radicals, and their structures were discussed in detail. The magnetic susceptibility measurements were carried out for the nine kinds of isolated radicals with a SQUID magnetometer. One radical showed ferromagnetic coupling ($2J/k_B$ = 44 K), and the others showed antiferromagnetic behavior. The magnetic interactions observed are explained on the basis of the crystal structures.

Introduction

Thioaminyls (RṄSR′) are electronically stabilized by the conjugative delocalization of the unpaired electron from nitrogen to sulfur.[2] In the continuing studies on thioaminyl radicals, we have found that a variety of 2,4,6-trisubstituted *N*-(arylthio)phenylaminyls[3−8] and *N*-(arylthio)-2-*tert*-butyl- and 2,7-di-*tert*-butyl-1-pyrenylaminyls[9] are persistent enough to be isolated. The typical features of thioarylaminyls are (1) their extensive π-electronic systems, (2) the convenient two-step syntheses of a variety of thioarylaminyls from the corresponding aromatic amines, and (3) their unreactivity with oxygen. Accordingly, thioarylaminyls can be expected as a spin source or as building blocks for organic magnets.[10,11]

The magnetic characterization of isolated thioarylaminyl radical crystals has shown that, although most radicals exhibited antiferromagnetic interactions, seven thioarylaminyls showed one-dimensional ferromagnetic interactions of $2J/k_B$ = 3.4−28.0 K,[5−8,12] which are much larger than those of nitroxides or nitronyl nitroxides having a localized π-spin system because thioarylaminyls have an extensive π-electronic conjugated system. However, the X-ray crystallographic analyses for the ferromagnetic radicals were unsuccessful because no single crystals suitable for X-ray crystallographic analysis could be obtained despite much effort. Therefore, we could not discuss the mechanism for the ferromagnetic interaction based on the crystal structures.

In the present work we prepared *N*-(2-pyridylthio)-2,6-diaryl-4-R-phenylaminyls (R = Ph, 4-ClC_6H_4, MeCO, CN, EtOCO; **1**) and *N*-(4-pyridylthio)-2,6-diaryl-4-R-phenylaminyls (R = Ph, 4-ClC_6H_4, EtOCO; **2**; Chart 1). Pyridyl-substituted thioarylaminyl radicals are expected to coordinate to transition-metal ions such as Cu(II) and Mn(II) to give transition-metal ion complexes. Fortunately, radicals **1** and **2** were quite persistent and could be successfully isolated as radical crystals. In the magnetic study of the isolated radicals, one radical was shown to couple ferromagnetically with an interaction of $2J/k_B$ = 44 K, and the ferromagnetic interaction could be explained on the basis of the X-ray crystallographic structure of the ferromagnetic radical. This is the first

* To whom correspondence should be addressed (Y.M.). Phone: +81-6-6605-2798. Fax: +81-6-6605-2769.

† Department of Applied Chemistry, Graduate School of Engineering.

‡ Department of Material Science and Chemistry, Graduate School of Science.

(1) ESR Studies of Nitrogen-Centered Free Radicals. 56. Part 55: Miura, Y.; Matsuba, N.; Tanaka, R.; Teki, Y. *J. Org. Chem*. **2002**, *25*, 8764.

(2) Miura, Y. *Trends in Org. Chem*. **1997**, *6*, 187; *Recent Res. Dev. Org. Chem*. **1998**, *2*, 251.

(3) Miura, Y.; Tanaka, A.; Hirotsu, K. *J. Org. Chem*. **1991**, *56*, 6638.

(4) Miura, Y.; Momoki, M.; Fuchikami, T.; Teki, Y.; Itoh, K.; Mizutani, H. *J. Org. Chem*. **1996**, *61*, 4300.

(5) Miura, Y.; Momoki, M.; Nakatsuji, M.; Teki, Y. *J. Org. Chem*. **1998**, *63*, 1555.

(6) Miura, Y.; Kurokawa, S.; Nakatsuji, M.; Ando, K.; Teki, Y. *J. Org. Chem*. **1998**, *63*, 8295.

(7) Miura, Y.; Tomimura, T.; Teki, Y. *J. Org. Chem*. **2000**, *65*, 7889.

(8) Nakatsuji, M.; Miura, Y.; Teki, Y. *J. Chem. Soc., Perkin Trans. 2* **2001**, 738.

(9) Miura, Y.; Yamano, E.; Tanaka, A.; Yamauchi, J. *J. Org. Chem*. **1994**, *59*, 3294. Miura, Y.; Yamano, E. *J. Org. Chem*. **1995**, *60*, 1070. Miura, Y.; Oka, H.; Yamano, E.; Teki, Y.; Takui, T.; Itoh, K. *Bull. Chem. Soc. Jpn*. **1995**, *68*, 1187.

(10) *Magnetic Properties of Organic Materials*; Lahti, P. M., Ed.; Marcel Dekker: New York, 1999.

(11) Proceedings of the 7th International Conference on Molecule-Based Magnets. *Polyhedron* **2001**, *20*, 1115−1784.

(12) Teki, Y.; Itoh, K.; Okada, A.; Yamakage, H.; Kobayashi, T.; Amaya, K.; Kurokawa, S.; Ueno, S.; Miura, Y. *Chem. Phys. Lett*. **1997**, *270*, 573.

10.1021/jo0205659 CCC: $25.00
Published on Web 01/22/2003

CHART 1

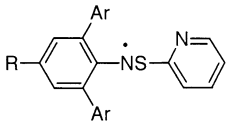

1

a: Ar = R = Ph
b: Ar = R = 4-ClC_6H_4
c: Ar = Ph, R = COMe
c-d_{10}: Ar = C_6D_5, R = COMe
d: Ar = 4-ClC_6H_4, R = COMe
e: Ar = Ph, R = CN
f: Ar = 4-ClC_6H_4, R = CN,
g: Ar = 4-ClC_6H_4, R = COOEt

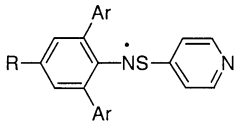

2

a: Ar = R = Ph
a-d_{15}: Ar = R = C_6D_5
b: Ar = R = 4-ClC_6H_4
c: Ar = 4-ClC_6H_4, R = COOEt

SCHEME 1

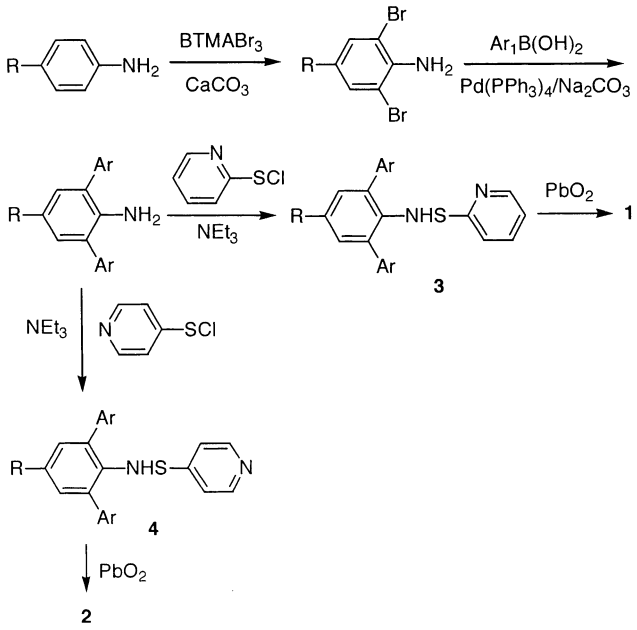

ferromagnetic thioaminyl radical that has an interaction that could be explained on the basis of the X-ray crystal structure. Herein we report the preparation, isolation, ESR spectra, spin-density calculations, X-ray crystallographic analyses, and magnetic characterization of **1** and **2**.

Results and Discussion

Preparation and Isolation of Radicals. 2,4,6-Trisubstituted *N*-(2-pyridylthio)anilines **3** and 2,4,6-trisubstituted *N*-(4-pyridylthio)anilines **4**, the corresponding precursors of **1** and **2**, were prepared according to Scheme 1. The reaction of 2,4,6-triarylanilines or 2,6-diaryl-4-R-anilines with 2- or 4-pyridinesulfenyl chloride in the presence of Et_3N gave **3a**−**g** in 30−69% and **4a**−**c** in 23−55% yields, respectively.

The oxidation of **3** and **4** was performed in benzene with PbO_2. This is the usual method for generation of thioarylaminyl radicals from the corresponding 2,4,6-trisubstituted *N*-(arylthio)anilines. When PbO_2 was added to a stirred solution of **3** or **4** in benzene, the initially colorless or light yellow solutions immediately turned green (**1b**), bluish green (**1c**, **1d**, **2b**), greenish blue (**1a**, **2a**), bluish purple (**1e**, **1g**), purplish blue (**1f**), or purple (**2c**) and the subsequent solutions showed an intense 1:1:1 triplet ESR signal. The UV−visible data and ESR parameters for **1** and **2** are summarized in Table 1.

TABLE 1. ESR and UV−Vis Spectrum Data for 1 and 2 in Benzene[a]

radical	a_N/mT[b,c]	g[c]	λ_{max}/nm (ϵ/L cm^{-1} mol^{-1})
1a	0.907	2.0055	621 (6290), 525 (2480 sh), 430 (6630 sh), 376 (19600), 335 (11900 sh)
1b	0.903	2.0057	630 (7160), 530 (2810 sh), 435 (8140 sh), 381 (24700), 350 (17000 sh)
1c	0.887	2.0059	623 (4430), 555 (3030), 426 (13600), 404 (11900), 374 (15300)
1c-d_{10}[d,e]	0.890	2.0059	
1d	0.881	2.0061	625 (4150), 558 (2810), 426 (12000), 403 (10800), 377 (14400)
1e	0.885	2.0059	619 (4810), 547 (3510), 416 (8290), 390 (12900 sh), 369 (16000)
1f	0.881	2.0061	625 (5020), 546 (3580), 417 (9060), 390 (11100 sh), 369 (16400)
1g	0.896	2.0061	614 (4400), 545 (3430), 416 (9850), 395 (11800 sh), 370 (15600)
2a	0.898	2.0055	
2a-d_{15}[d,f]	0.899	2.0055	
2b	0.897	2.0057	627 (7260), 535 (2850 sh), 435 (7760 sh), 384 (25500)
2c	0.890	2.0061	606 (4350), 544 (3460), 415 (10500 sh), 372 (17000)

[a] Measured at room temperature (ca. 20 °C). [b] a_N for the NS nitrogen. [c] The nitrogen and proton hfc constants and g values are determined by comparison with Fremy's salt in an aqueous dilute K_2CO_3 solution (a_N = 1.309 mT, g = 2.0057). [d] The hfc constants are determined by computer simulation. [e] a_H(anilino meta protons) = 0.140 (2H), a_H(H-3 and H-5 of the 2-pyridine ring) = 0.090 (2H), a_N(2-pyridyl nitrogen) = 0.047 mT. [f] a_H(anilino meta protons) = 0.137 (2H), a_H(H-3 and H-5 of the 4-pyridine ring) = 0.078 (2H), a_N(4-pyridyl nitrogen) = 0.043 mT.

All radicals generated were quite persistent, and no reaction with atmospheric oxygen was observed. The oxygen-inert property of **1** and **2** is characteristic of thioarylaminyl radicals. The radicals generated were isolated according to the previously reported method.[3−9] That is, the oxidation of **3** and **4** with PbO_2 in benzene, removal of the solvent by the freeze-drying method, and subsequent recrystallization from hexanes−ethyl acetate gave black, blue, green, or purple crystals in 24−44% yields. The only exception was **2a**. Although this radical was very persistent, similar to the other thioaminyls, it never crystallized despite much effort.

The structures of the isolated radicals were confirmed by IR and elemental analyses. The IR spectra showed the complete disappearance of the peak due to the ν around 3320 cm^{-1} (NH), and the elemental analyses gave satisfactory agreement with the calculations. Furthermore, the structures of **1a**, **1c**, and **1e** were later confirmed by single-crystal X-ray crystallographic analyses. The purities of the isolated radical crystals determined by the magnetic susceptibility measurements were >95%, as described below.

ESR Spectra. ESR spectra were measured at room temperature (ca. 20 °C) using benzene as the solvent. A typical ESR spectrum is shown in Figure 1. All the radicals measured showed a broad 1:1:1 triplet ESR spectrum with a large line width (ΔH_{pp}) of about 0.3 mT, as shown in Figure 1, and no hyperfine couplings due to the aromatic protons or the pyridyl nitrogen were observed. This is due to the presence of many aromatic protons with unresolved, small hyperfine coupling (hfc)

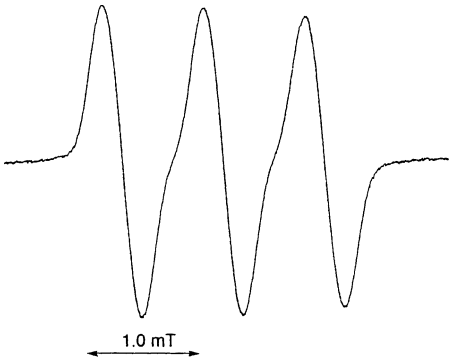

FIGURE 1. ESR spectrum of **1a** in benzene at 20 °C.

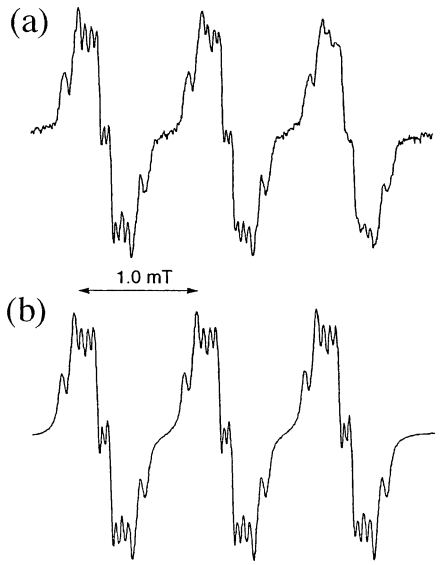

FIGURE 2. ESR spectrum of **1c**-d_{10} in benzene at 20 °C: (a) observed spectrum; (b) computer simulation.

constants. The unresolved, small couplings due to the aromatic protons can be removed by the deuteration of the benzene rings attached at the 2, 4, and 6 positions of the anilino groups. Such partially deuterated thioaminyl radicals, **1c**-d_{10} and **2a**-d_{15}, were prepared from the corresponding deuterated phenyl-substituted anilines, according to the same procedures as those for the corresponding nondeuterated thioaminyls. As a typical example, an ESR spectrum of **1c**-d_{10} is shown in Figure 2, together with a computer simulation. Although the resolution of the spectrum is still poor, the computer-simulated spectrum reconstructs well the experimental one by using the following hfc constants: $a_N = 0.890$ (NS) and 0.047 (pyridyl N) mT and $a_H = 0.140$ (anilino meta H) and 0.090 (2-pyridyl 3- and 5-H) mT. A very similar ESR spectrum was also obtained for **2a**-d_{15}, and the computer simulation gave $a_N = 0.899$ (NS) and 0.043 (4-pyridyl N) mT and $a_H = 0.137$ (anilino meta H) and 0.078 (4-pyridyl 3- and 5-H) mT.

X-ray Crystallographic Analyses. Upon recrystallization from hexanes−ethyl acetate, single crystals suitable for X-ray crystallographic analysis were obtained for **1a**, **1c**, and **1e**, and this led to the successful X-ray crystallographic analyses. The Oak Ridge thermal ellipsoid plot (ORTEP) drawings are shown in Figures 3−5, and selected bond lengths and angles and torsion angles

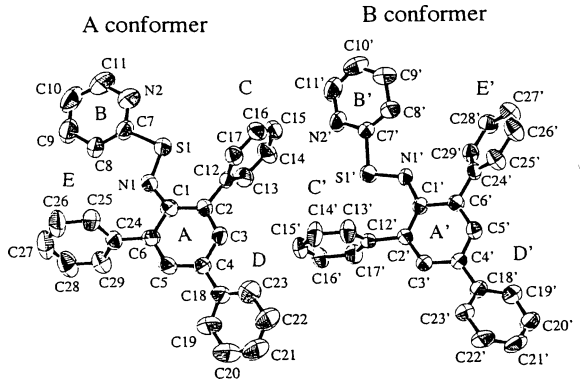

FIGURE 3. ORTEP drawing of radical **1a**.

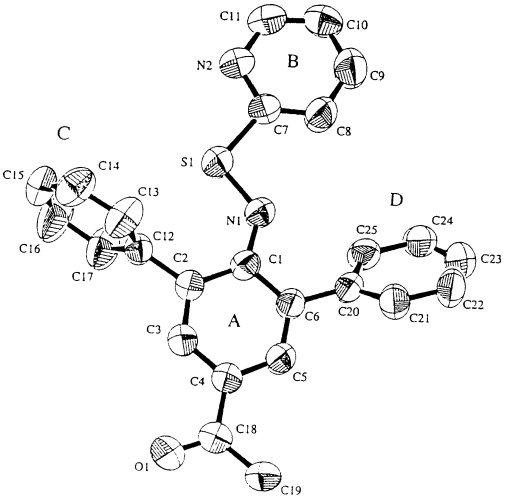

FIGURE 4. ORTEP drawing of radical **1c**.

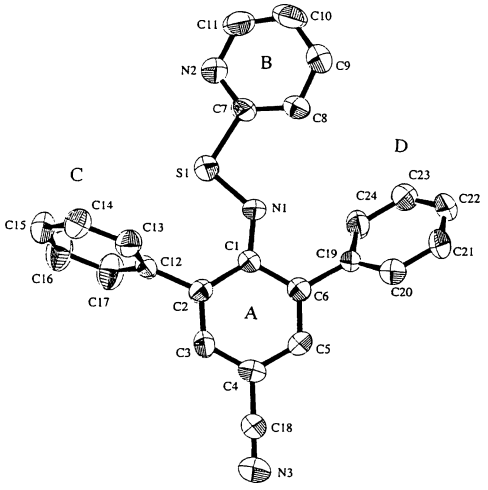

FIGURE 5. ORTEP drawing of radical **1e**.

are summarized in Table 2. Radical **1a** was shown to have two conformers in crystal, and **1c** showed that ring C is disordered over two sites with an occupancy of 0.5 and 0.5. One (C20−C25) is twisted by 132.3° from ring A, and the other (C20−C26−C27−C23−C28−C29) is twisted by 48.5°. In Figure 4, only one comformer is shown for clarity.

Table 2 shows that the three radicals have a similar bond length with respect to the C1−N1 and S1−C7

TABLE 2. Selected Bond Lengths and Bond and Torsion Angles for 1a, 1c, and 1e

radical	bond length/Å		bond angle/deg		torsion angle/deg	
1a	C1−N1	1.368(8)	C1−N1−S1	124.8(5)	S1−N1−C1−C2	−2.8(9)
	(C1′−N1′)	[1.364(8)]	(C1′−N1′−S1′)	[125.1(5)]	(S1′−N1′−C1′−C2′)	[−18.2(8)]
	N1−S1	1.630(6)	N1−S1−C7	99.3(4)	S1−N1−C1−C6	179.6(4)
	(N1′−S1′)	[1.622(5)]	(N1′−S1′−C7′)	[99.7(4)]	(S1′−N1′−C1′−C6′)	[165.7(4)]
	S1−C7	1.780(8)	N1−C1−C2	128.9(6)	C1−N1−S1−C7	178.6(5)
	(S1′−C7′)	[1.781(7)]	(N1′−C1′−C2′)	[128.5(6)]	(C1′−N1′−S1′−C7′)	[178.0(4)]
			N1−C1−C6	112.7(6)	N1−S1−C7−C8	−6.2(7)
			(N1′−C1′−C6′)	[113.6(6)]	(N1′−S1′−C7′−C8′)	[−4.8(6)]
					N1−S1−C7−N2	177.2(5)
					(N1′−S1′−C7′−N2′)	[177.9(5)]
1c	C1−N1	1.372(4)	C1−N1−S1	125.7(3)	S1−N1−C1−C2	−0.7(5)
	N1−S1	1.601(3)	N1−S1−C7	100.9(2)	S1−N1−C1−C6	176.6(3)
	S1−C7	1.775(4)	N1−C1−C2	126.9(3)	C1−N1−S1−C7	−177.8(3)
			N1−C1−C6	114.5(3)	N1−S1−C7−N2	176.3(3)
					N1−S1−C7−C8	−5.0(4)
1e	C1−N1	1.361(6)	C1−N1−S1	126.7(5)	S1−N1−C1−C2	−15.5(9)
	N1−S1	1.599(4)	N1−S1−C7	99.5(3)	S1−N1−C1−C6	166.4(4)
	S1−C7	1.770(6)	N1−C1−C2	127.3(7)	C1−N1−S1−C7	−177.9(5)
			N1−C1−C6	116.3(6)	N1−S1−C7−N2	172.1(5)
					N1−S1−C7−C8	−9.6(6)

SCHEME 2

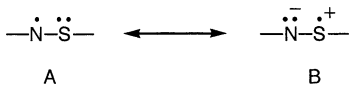

bonds, while the N−S bond lengths vary in the range from 1.599(4) (**1e**) to 1.630(6) (**1a**) Å, depending on the electronic nature of the para substituent. That is, the electron-withdrawing substituents (MeCO and CN) shorten the N−S bond by 0.021−0.031 Å compared with that of the phenyl-substituted radical, **1a**. On the other hand, the C1−N1−S1 and N1−S1−C7 bond angles are constant within the experimental errors.

Thioaminyl radicals are represented by two canonical forms, A and B (Scheme 2). Electron-withdrawing substituents such as MeCO and CN enhance the relative importance of canonical form B, while electron-donating substituents enhance the relative importance of canonical form A. Enhancement of the ionic form B shortens the N−S bond, while enhancement of the neutral form A lengthens the N−S bond.[13] As for the substitution effect on a_N, enhancement of the neutral form A will increase a_N (because of the NS nitrogen), while enhancement of the ionic form B will decrease a_N. This substituent effect on a_N is clearly observed in Table 1. That is, the radicals bearing electron-withdrawing substituents such as **1c**−**g** and **2c** show relatively small a_N's, while the phenyl- or 4-chlorophenyl-substituted radicals such as **1a**, **1b**, **2a**, and **2b** give relatively large a_N's.

A notable difference between the two conformers **1a**-A and **1a**-B is found in the planarity of the phenyl−N−S−pyridyl π framework. While conformer **1a**-A adopts a planar phenyl−N−S−pyridyl π framework, that of **1a**-B is less planar; namely, in **1a**-A the N and S atoms are coplanar with ring A within 0.031 Å, and this plane makes a dihedral angle of 7.5° with ring B. On the other hand, **1a**-B shows a large torsion angle of −18.2(8)° for S1′−N1′−C1′−C2′ [165.7(4)° for S1′−N1′−C1′−C6′]. The dihedral angles between rings A and C, between rings A and D, and between rings A and E are 86.1, 28.1, and 61.3°, respectively, and those between rings A′ and C′, between rings A′ and D′, and between rings A′ and E′ are 82.1, 35.4, and 49.8°, respectively, indicating that there is a large steric congestion around the radical center in both conformers.

Radical **1c** showed a planar phenyl−N−S−pyridyl π framework. That is, the N and S atoms are coplanar with ring A within 0.037 Å, and this plane makes a dihedral angle of 6.1°. The dihedral angles between rings A and C and between rings A and D are 82.2 and 47.7° (or 48.5° for the disorder), again indicating that there is a large steric congestion around the radical center, similar to that of **1a**.

Radical **1e** shows a relatively large torsion angle of −15.5(9)° for S1−N1−C1−C2 [166.4(4)° for S1−N1−C1−C6], revealing that the phenyl−N−S−pyridyl π framework is not planar. The dihedral angles between rings A and C and between rings A and D are 75.1 and 48.6°, respectively, which are similar to those of the above radicals.

Spin-Density Calculations. The ab initio molecular orbital (MO) calculations based on the density functional theory (DFT) were performed for **1a**, **1c**, **1e**, and **2a** by the UBecke 3LYP hybrid method using the STO 6-31G basis set. All the calculations were carried out on Gaussian 98.[14] The MO calculations of **1a**, **1c**, and **1e** were performed using the X-ray crystallographic structures. The total atomic spin densities in **1c** are shown in Figure 6, and the calculated hfc constants are compared with the experimentally determined hfc constants in Table 3.

(13) Fu, Y.; Lin, B.-L.; Song, K.-S.; Liu, L.; Guo, Q.-X. *J. Chem. Soc., Perkin Trans. 2* **2002**, 1231.

(14) All calculations were carried out on Gaussian 98W (Revision A.9). Frisch, M. J.; Trucks, G. W.; Schlegel, H. B.; Scuseria, G. E.; Robb, M. A.; Cheeseman, J. R.; Zakrzewski, V. G.; Montgomery, J. A., Jr.; Stratmann, R. E.; Burant, J. C.; Dapprich, S.; Millam, J. M.; Daniels, A. D.; Kudin, K. N.; Strain, M. C.; Farkas, O.; Tomasi, J.; Barone, V.; Cossi, M.; Cammi, R.; Mennucci, B.; Pomelli, C.; Adamo, C.; Clifford, S.; Ochterski, J.; Petersson, G. A.; Ayala, P. Y.; Cui, Q.; Morokuma, K.; Malick, D. K.; Rabuck, A. D.; Raghavachari, K.; Foresman, J. B.; Cioslowski, J.; Ortiz, J. V.; Baboul, A. G.; Stefanov, B. B.; Liu, G.; Liashenko, A.; Piskorz, P.; Komaromi, I.; Gomperts, R.; Martin, R. L.; Fox, D. J.; Keith, T.; Al-Laham, M. A.; Peng, C. Y.; Nanayakkara, A.; Challacombe, M.; Gill, P. M. W.; Johnson, B.; Chen, W.; Wong, M. W.; Andres, J. L.; Gonzalez, C.; Head-Gordon, M.; Replogle, E. S.; Pople, J. A. Gaussian 98W, Revision A.9; Gaussian, Inc.: Pittsburgh, PA, 1998.

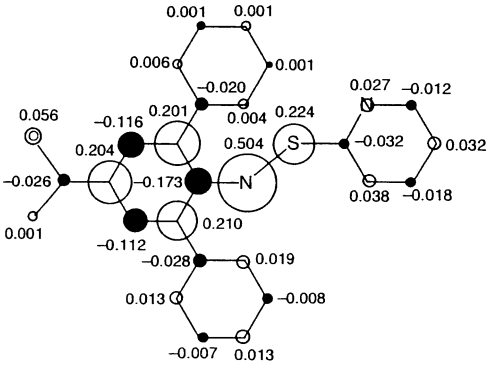

FIGURE 6. The total atomic spin densities for **1c**. The spin-density calculations based on the DFT were performed at the UBecke 3LYP/STO 6-31G level.

TABLE 3. Calculated hfc Constants of 1c

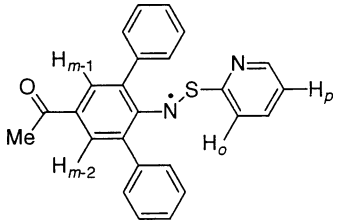

position	calcd hfc const[a,b]	obsd hfc const for **1c**[a,c]	obsd hfc const for **1c**-d_{10}[a,c]
N1[d]	1.212	0.887	0.890
$H_{m\text{-}1}$	0.191		0.140
$H_{m\text{-}2}$	0.177		0.140
H_o	−0.089		0.090
H_p	−0.076		0.090
N2[e]	0.039		0.047

[a] The hfc constants are given in mT. [b] The hfc constants were calculated at the DFT UBecke 3LYP/STO 6-31G level. [c] The hfc constants are shown in the absolute values. [d] Refers to the NS nitrogen. [e] Refers to the 2-pyridyl nitrogen.

Although a somewhat large discrepancy in the hfc constant is found for the NS nitrogen, excellent agreements between the observations and the calculations were obtained for the other hfc constants, indicating that the MO calculations performed at the DFT UBecke 3LYP/STO 6-31G level afford reliable results and strongly support the ESR results indicating that the unpaired electron spin mainly resides on the NS nitrogen, sulfur, and anilino benzene ring. Such a spin-density distribution is essentially the same as those for the previously reported 2,4,6-trisubstituted *N*-(arylthio)phenylaminyls.

We also note the pyridyl-nitrogens' hfc constants because the magnetic behavior of their transition-metal complexes is governed by the spin density on the pyridyl nitrogen. The hyperfine splittings due to the pyridyl nitrogen were observed for **1c**-d_{10} and **2a**-d_{15}. The calculated nitrogen hfc constant of 0.039 mT for **1c**-d_{10} is in good agreement with the observed value of 0.047 mT, predicting the spin density of 0.027 for the pyridyl nitrogen. A similar nitrogen hfc constant of 0.043 mT was also observed for the pyridyl nitrogen of **2a**-d_{15}. From these ESR and calculated results, we can expect to observe the magnetic interactions between the radicals and metals when the transition-metal ion complexes of **1** or **2** are prepared.

TABLE 4. Magnetic Behavior of 1 and 2 in Crystal

radical	$2J/k_B$/K	α	model used for analyses[a]
1a	−151[b]	0.80	a
1b	−122		b
1c	−34		c
1d	$\theta = -0.91$		d
1e	44		c
1f	−14	0.87	a
1g	−65	0.88	a
2b	−24		c
2c	−39	0.27	a

[a] Models: (a) one-dimensional alternating model; (b) dimer model; (c) one-dimensional Heisenberg model; and (d) Curie−Weiss low. [b] The theoretical curve is drawn by eq 2 on the assumption that **1a**-A contacts antiferromagnetically between the neighboring radical molecules and **1a**-B is paramagnetic.

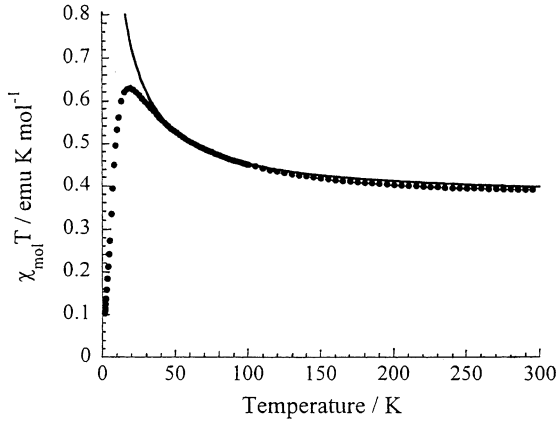

FIGURE 7. $\chi_{mol}T$ versus T plots of **1e**. The solid theoretical curve was calculated by the one-dimensional Heisenberg model with $2J/k_B = 44$ K.

Magnetic Susceptibility Measurements. The magnetic susceptibility (χ) measurements for the isolated radical crystals were carried out using polycrystalline samples with a SQUID magnetometer in the temperature range 1.8−300 K. The diamagnetic components were subtracted by the estimation based on Pascal's sum rule. The results of the magnetic susceptibility measurements are summarized in Table 4.

Figure 7 shows $\chi_{mol}T$ versus T plots for **1e** (where χ_{mol} is the molar magnetic susceptibility). The $\chi_{mol}T$ value increases with decreasing temperature and below 20 K drastically decreases with decreasing temperature. Such a magnetic behavior suggests that the intrachain interaction is ferromagnetic and the interchain interaction is antiferromagnetic. An analysis with the one-dimensional regular Heisenberg model[15] (eq 1) gave $2J/k_B = 44$ K as

$$H = -2J\sum \mathbf{S}_i \cdot \mathbf{S}_j \qquad (1)$$

the intrachain ferromagnetic interaction. To clarify the ferromagnetic mechanism, the crystal structure of **1e** (Figure 8) was carefully surveyed. The radical molecules are stacked along the *c* axis. The nearest contacts between the neighboring radical molecules are found for S1- - -C7′ and C7- - -S1′. For S1- - -C7′ and C7- - -S1′, two kinds of distances, 3.79 and 3.90 Å, were observed, as

(15) Bonner, J. C.; Fisher, M. E. *Phys. Rev.* **1964**, *A135*, 640.

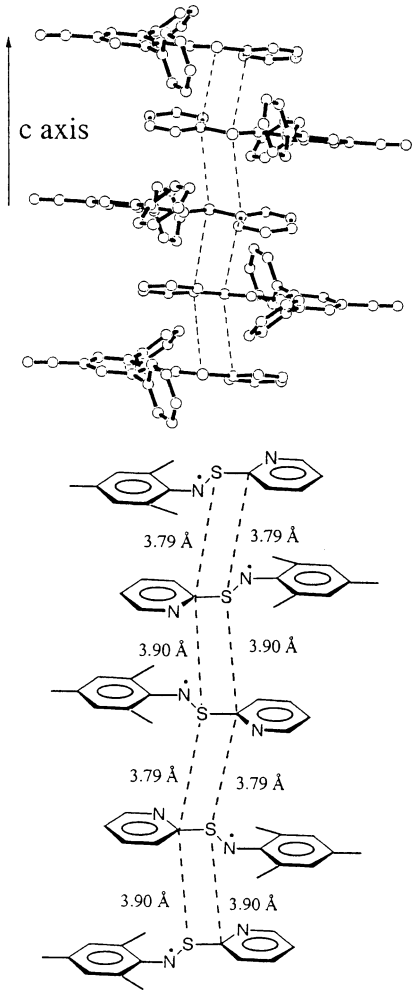

FIGURE 8. Crystal structure of **1e** and a schematic illustration of the crystal structure showing the magnetic interaction.

found in Figure 8. According to the McConnell rule,[16] the signs of the spin densities between S1 and C7′ and between C7 and S1′ are opposite to each other and such contacts through S1- - -C7′ and C7- - -S1′ yields a ferromagnetic interaction between the neighboring radical molecules. The MO calculations for **1e** based on the DFT UBecke 3LYP hybrid method predict that the spin density on C7 is −0.033 and that on S is 0.221. Although the spin density on C7 is low, that on S is high. The strong ferromagnetic interaction of $2J/k_B = 44$ K can therefore be explained in terms of the high spin density on sulfur. Furthermore, the large sulfur 3p orbital must contribute to such a strong ferromagnetic interaction because the large orbital is favorable to the overlapping of the orbitals between the neighboring radical molecules. Although we previously found eight ferromagnetic thioaminyls,[4−8,12] we were unsuccessful in their X-ray crystallographic analyses because of their poor crystal qualities. Accordingly, **1e** is the first ferromagnetic thioaminyl whose magnetic interaction could be explained on the basis of the X-ray crystallographic results.

On the other hand, radicals **1b**, **1c**, **1d**, **1f**, **1g**, **2b**, and **2c** showed antiferromagnetic interaction. In Figure 9, the $\chi_{mol}T$ versus T plots for **1c** are depicted. Analysis of the

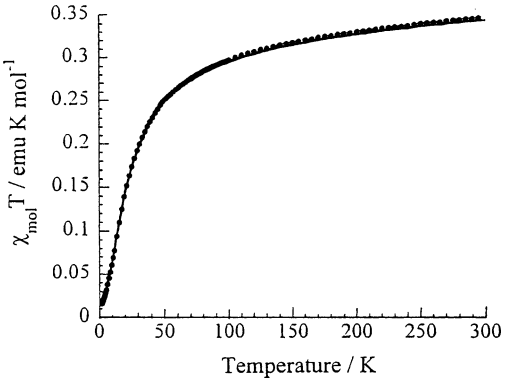

FIGURE 9. $\chi_{mol}T$ versus T plots of **1c**. The solid theoretical curve was calculated by the one-dimensional regular Heisenberg model with $2J/k_B = -34$ K.

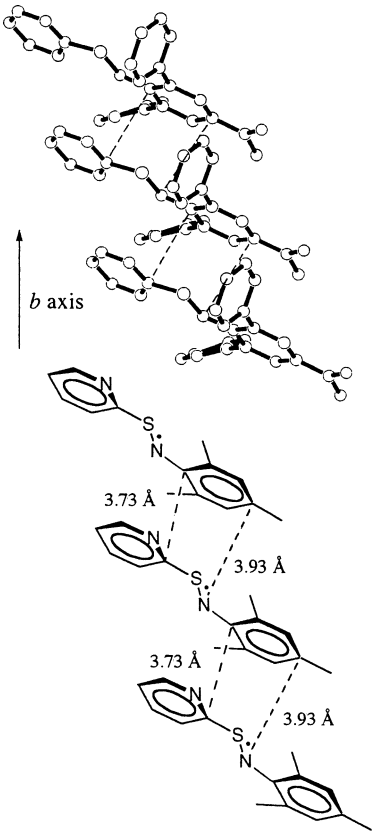

FIGURE 10. Crystal structure of **1c** and a schematic illustration of the crystal structure showing the magnetic interaction.

$\chi_{mol}T$ versus T plots with the one-dimensional regular Heisenberg model (eq 1) gave $2J/k_B = -34$ K. In Figure 10, the crystal structure of **1c** is shown. The radical molecules are stacked along the *b* axis, and the intermolecular interactions take place through the N1- - -C4′ (3.93 Å) and C1- - -C7′ (3.73 Å) contacts. According to the McConnell rule, the signs of the spin densities between N1 and C4′ and between C1 and C7′ are opposite to each other, and from this rule the interactions through the N1- - -C4′ and C1- - -C7′ contacts between the neighboring radical molecules are shown to be antiferromagnetic. The MO calculations by the DFT UBecke 3LYP method predict that the spin densities on N1, C4, C1, and C7 are 0.504, 0.204, −0.173, and −0.032, respectively,

(16) McConnell, H. M. *J. Chem. Phys.* **1963**, *39*, 1910.

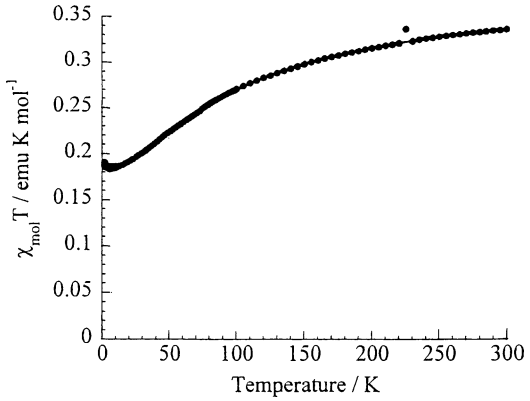

FIGURE 11. $\chi_{mol}T$ versus T plots for **1a**. The theoretical solid curve is obtained on the assumption that the interaction within the columns consisting of **1a**-A is antiferromagnetic ($2J/k_B = -151$ K and $\alpha = 0.80$) and within the columns consisting of **1a**-B the radical molecules are paramagnetic.

indicating that the spin densities on N1, C4, and C1 are high, while that on C7 is very low. Accordingly, it is obvious that the observed intrachain antiferromagnetic interaction takes place mainly through the N1- - -C4′ contact.

Radical **1a** showed an unusual magnetic behavior. In Figure 11, the $\chi_{mol}T$ versus T plots are depicted. The $\chi_{mol}T$ value decreases monotonously with decreasing temperature. However, different from the usual antiferromagnetic radicals, the $\chi_{mol}T$ value does not fall to ∼0 emu K mol^{-1} at 0 K. The $\chi_{mol}T$ at 0 K is 0.185 emu K mol^{-1}, which is just half the Curie constant (0.376 emu K mol^{-1}) for the paramagnetic $S = {}^1/_2$ spin system. One possible explanation for the unusual magnetic behavior is based on the X-ray crystallographic result that radical **1a** adopts two kinds of conformers in crystal: one conformer interacts antiferromagnetically with the neighboring radical molecules, and the other conformer has no interaction with the neighboring radical molecules, namely, paramagnetic. To solve this unusual magnetic behavior, we surveyed carefully the crystal structure of **1a** depicted in Figure 12. The radical molecules are stacked along the *c* axis and have two kinds of columns. One column is constituted of the **1a**-A conformers alone, and the other is constituted of the **1a**-B conformers alone. In the former column, **1a**-A interacts with the neighboring radical molecules with the shortest distance of 3.80 Å for S1- - -C4′. The second shortest contact is observed for S1- - -C3′, whose distance is 3.93 Å. According to the McConnell rule, the contact through S1- - -C4′ yields an antiferromagnetic interaction for the neighboring radical molecules and the contact through S1- - -C3′ affords a ferromagnetic interaction. The MO calculations based on the DFT UBecke 3LYP method predict that the spin densities on S1, C4′, and C3′ are 0.171, 0.265, and −0.129, respectively. Because the spin density on C4 is higher than that on C3 and the N1- - -C4′ distance is shorter than the N1- - -C3′ distance, the antiferromagnetic interaction through the S1- - -C4′ contact must dominate over the ferromagnetic interaction through the S1- - -C3′ contact. In the column consisting of **1a**-B conformers, **1a**-B interacts with the neighboring radical molecules with the shortest distance of 3.92 Å for S1′- - -(C3′)′. The second shortest contact is found for S1′- - -(C4′)′, whose distance is 4.13 Å. According to the McConnell rule, the contact through S1′- - -(C3′)′ yields a ferromagnetic interaction, while the contact through S1′- - -(C4′)′ affords an antiferromagnetic interaction. The MO calculations based on the DFT Ubecke 3LYP method predict that the spin densities on S1′, C3′, and C4′ are 0.161, −0.108, and 0.217, respectively. Although the S1′- - -(C3′)′ distance is shorter than that for the S1′- - -(C4′)′ distance, the spin density on C3′ is much lower than that on C4′. If the ferromagnetic interaction through the S1′- - -(C3′)′ contact and the antiferromagnetic interaction through the S1′- - -(C4′)′ contact balance with each other, the magnetic interaction between the neighboring radicals, namely, paramagnetic, will apparently disappear. On the basis of the X-ray crystallographic results, the $\chi_{mol}T$ plots shown in Figure 11 were analyzed by the sum of the two components showing different magnetic behavior given by eq 2a.

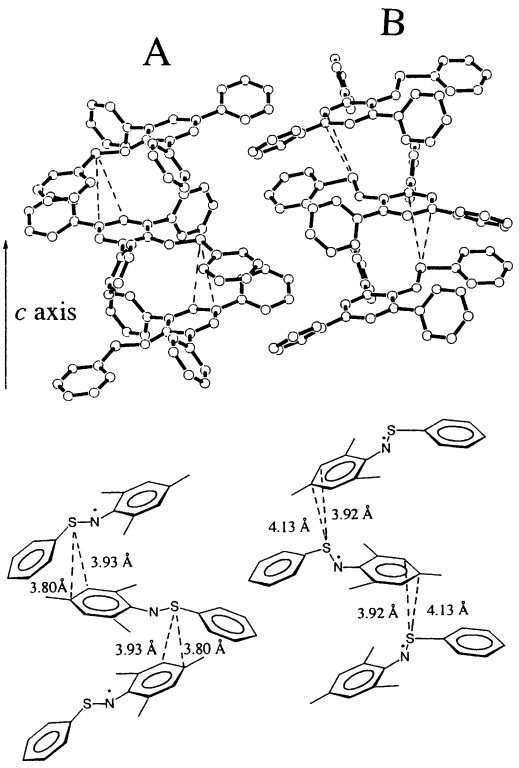

FIGURE 12. Crystal structure of **1a** and a schematic illustration of the crystal structure showing the magnetic interaction: (A) crystal structure of conformer **1a**-A and (B) crystal structure of conformer **1a**-B.

$$\chi_{mol} = (\chi_{mol}^{1D\ alt} + \chi_{mol}^{para})/2 \qquad (2a)$$

Here, $\chi_{mol}^{1D\ alt}$ is the magnetic susceptibility of the one-dimensional chain for **1a**-A represented by eq 2b.[17,18]

$$H = -2J\sum(\mathbf{S}_{2i}\cdot\mathbf{S}_{2i-1} + \alpha\mathbf{S}_{2i}\cdot\mathbf{S}_{2i+1}) \qquad (2b)$$

χ_{mol}^{para} is the Curie paramagnetic component (C/T, $C =$ 0.376 emu K mol^{-1}) arising from the noninteracting column of **1a**-B. When $2J/k_B$ was −150.6 K and α

(17) Duffy, W., Jr.; Barr, K. P. *Phys. Rev.* **1968**, *165*, 647.
(18) Hall, J. W.; March, E. W.; Weller, R. R.; Hatfield, W. E. *Inorg. Chem.* **1981**, *20*, 1033.

(alternating parameter) was 0.80, a satisfactory agreement with the experimental results was observed, as found in Figure 11. Although the X-ray crystallographic results showed a uniform chain structure, the magnetic behavior was best analyzed by using the alternating model with $\alpha = 0.80$. This discrepancy may be explained in terms of the breaking of the uniform chain structure of the crystal at low temperature.

The reactions of **1** or **2** with Mn(II)(hfac)$_2$ or Cu(II)(hfac)$_2$ were attempted according to the literature procedure.[19] Although the reaction of **1** with Mn(II)(hfac)$_2$ or Cu(II)(hfac)$_2$ gave no desired complexes, the reaction of **2** with Mn(II)(hfac)$_2$ or Cu(II)(hfac)$_2$ afforded 2:1 complexes of **2** and Mn(II)(hfac)$_2$ or Cu(II)(hfac)$_2$. The magnetic studies and X-ray crystallographic analyses of the metal complexes obtained are underway. The results will be published elsewhere.

Conclusions

In the present study, 2,4,6-trisubstituted *N*-(2-pyridylthio)arylaminyls (**1**) and *N*-(4-pyridylthio)arylaminyls (**2**) were prepared and isolated as radical crystals. The spin-density calculations at the DFT UBecke 3LYP/STO 6-31G level gave excellent agreements with the experimental hfc constants and predicted that the unpaired electron spin resides mainly on the nitrogen, sulfur, and anilino benzene ring. The magnetic characterizations of the isolated radicals were carried out with a SQUID magnetometer. Although most radicals showed antiferromagnetic interactions, **1e** was ferromagnetic, and an analysis with the one-dimensional regular Heisenberg model gave $2J/k_B = 44$ K. The crystal structure of **1e** showed that the strong intrachain ferromagnetic interaction is due to the contact through S- - -C7′. The unusual antiferromagnetic behavior of **1a** was explained by its X-ray crystallographic results showing the presence of two kinds of columns that are magnetically different; namely, one is antiferromagnetic and the other is paramagnetic.

Experimental Section

IR, ^{1}H NMR, UV−vis, and ESR spectra were recorded as previously reported.[3−9] Magnetic susceptibility (χ) measurements were carried out in the temperature range 1.8−300 K with a SQUID magnetometer using a polycrystalline sample. Alumina column chromatography was carried out on Merck aluminum oxide 90.

Materials. 2,4,6-Tris(4-chlorophenyl)aniline,[20,21] 4-acetyl-2,6-diphenylaniline,[5] 4-acetyl-2,6-bis(4-chlorophenyl)aniline,[5] 4-cyano-2,6-diphenylaniline,[5] 4-ethoxycarbonyl-2,6-bis(4-chlorophenyl)aniline,[5,20] 2,4,6-tri(phenyl-d_5)aniline,[3,7,20] and 4-acetyl-2,6-di(phenyl-d_5)aniline[5] were obtained as previously reported. 2-Pyridine- and 4-pyridinesulfenyl chlorides were obtained by bubbling Cl_2 gas into a CH_2Cl_2 (20 mL) solution of 2,2′- or 4,4′-dipyridyl disulfide (1.54 g, 7.0 mmol) at room temperature for about 1 min. The further bubbling of Cl_2 yielded an insoluble material. The resulting light red solution, containing a small amount of insoluble materials, was concentrated to about 5 mL by bubbling N_2. The sulfenyl chloride solutions were used in the next reaction without further purification.

4-Cyano-2,6-bis(4-chlorophenyl)aniline. This compound was prepared by the Pd-catalyzed cross-coupling reaction of 2,6-dibromo-4-cyanoaniline with 3 equiv of 4-chlorophenylboronic acid by the usual procedure:[21,22] colorless prisms; mp 187−189 °C (ethanol); yield 84%; ^{1}H NMR ($CDCl_3$) δ 4.26 (s, 2H), 7.35 (s, 2H), 7.38 (d, $J = 8.3$ Hz, 4H), 7.47 (d, $J = 8.3$ Hz, 4H). Anal. Calcd for $C_{19}H_{12}Cl_2N_2$: C, 67.27; H, 3.57; N, 8.26. Found: C, 67.25; H, 3.67; N, 7.94.

General Procedure for the Preparation of 3. To a stirred solution of an aniline (7.0 mmol) and Et_3N (4 mL, 29 mmol) in dry ether (300 mL) was added a solution of 2-pyridinesulfenyl chloride (14 mmol) in CH_2Cl_2 (10 mL) dropwise at 0 °C. After completion of the addition, the mixture was stirred at 0 °C for 2 h and filtered. After filtration and evaporation, the residue was column chromatographed on alumina at 0 °C with 3:1 benzene−hexane (**3a**, **3b**, **3e**, **3g**) or benzene (**3c**, **3d**, **3f**) as the eluant. Crystallization from hexanes−ethyl acetate gave pure crystals.

***N*-(2-Pyridylthio)-2,4,6-triphenylaniline (3a):** yield 66%; colorless prisms; mp 108−110 °C; IR (KBr) 3330 (NH) cm^{-1}; ^{1}H NMR (acetone-d_6) δ 6.10 (br s, 1H), 6.81 (d, $J = 8.3$ Hz, 1H), 6.87 (dd, $J = 8.3$ and 4.9 Hz, 1H), 7.31−7.48 (m, 10H), 7.50 (s, 2H), 7.62 (d, $J = 7.8$ Hz, 4H), 7.72 (d, $J = 7.3$ Hz, 2H), 8.09 (d, $J = 4.9$ Hz, 1H). Anal. Calcd for $C_{29}H_{22}N_2S$: C, 80.90; H, 5.15; N, 6.51. Found: C, 80.65; H, 5.06; N, 6.45.

***N*-(2-Pyridylthio)-2,4,6-tris(4-chlorophenyl)aniline (3b):** yield 46%; colorless needles; mp 162−165 °C; IR (KBr) 3320 (NH) cm^{-1}; ^{1}H NMR (acetone-d_6) δ 6.20 (br s, 1H), 6.90−6.95 (m, 2H), 7.42−7.47 (m, 7H), 7.51 (s, 2H), 7.60 (d, $J = 8.3$ Hz, 4H), 7.76 (d, $J = 8.3$ Hz, 2H), 8.14 (d, $J = 4.9$ Hz, 1H). Anal. Calcd for $C_{29}H_{19}Cl_3N_2S$: C, 65.24; H, 3.59; N, 5.25. Found: C, 65.49; H, 3.67; N, 5.12.

***N*-(2-Pyridylthio)-4-acetyl-2,6-diphenylaniline (3c):** yield 44%; colorless prisms; mp 125−126 °C; IR (KBr) 3300 (NH) and 1670 (C=O) cm^{-1}; ^{1}H NMR (acetone-d_6) δ 2.56 (s, 3H), 6.37 (br s, 1H), 6.84 (d, $J = 8.3$ Hz, 1H), 6.90 (dd, $J = 7.3$ and 4.9 Hz, 1H), 7.37 (t, $J = 8.3$ Hz, 2H), 7.42−7.48 (m, 5H), 7.56 (d, $J = 8.3$ Hz, 4H), 7.79 (s, 2H), 8.11 (d, $J = 4.9$ Hz, 1H). Anal. Calcd for $C_{25}H_{20}N_2OS$: C, 75.73; H, 5.08; N, 7.07; Found: C, 75.92; H, 5.14; N, 6.72.

***N*-(2-Pyridylthio)-4-acetyl-2,6-bis(4-chlorophenyl)-aniline (3d):** yield 45%; colorless prisms; mp 132−134 °C; IR (KBr) 3340 (NH) and 1680 (C=O) cm^{-1}; ^{1}H NMR (acetone-d_6) δ 2.56 (s, 3H), 6.46 (br s, 1H), 6.92−6.98 (m, 2H), 7.46 (d, $J = 8.3$ Hz, 4H), 7.50 (t, $J = 7.8$ Hz, 1H), 7.56 (d, $J = 8.3$ Hz, 4H), 7.79 (s, 2H), 8.16 (d, $J = 4.9$ Hz, 1H). Anal. Calcd for $C_{25}H_{18}Cl_2N_2OS$: C, 64.52; H, 3.90; N, 6.02. Found: C, 64.73; H, 4.00; N, 5.78.

***N*-(2-Pyridylthio)-4-cyano-2,6-diphenylaniline (3e):** yield 36%; colorless prisms; mp 98−100 °C; IR (KBr) 3320 (NH) and 2230 (C≡N) cm^{-1}; ^{1}H NMR (acetone-d_6) δ 6.47 (br s, 1H), 6.84 (d, $J = 8.3$ Hz, 1H), 6.93 (dd, $J = 8.3$ and 4.9 Hz, 1H), 7.40 (t, $J = 8.3$ Hz, 2H), 7.45−7.49 (m, 5H), 7.53 (s, 2H), 7.56 (d, $J = 8.3$ Hz, 4H), 8.12 (d, $J = 4.9$ Hz, 1H). Anal. Calcd for $C_{24}H_{17}N_3S$: C, 75.96; H, 4.52; N, 11.07. Found: C, 75.59; H, 4.41; N, 10.94.

***N*-(2-Pyridylthio)-4-cyano-2,6-bis(4-chlorophenyl)-aniline (3f):** yield 66%; colorless prisms; mp 152−154 °C; IR (KBr) 3350 (NH) and 2230 (C≡N) cm^{-1}; ^{1}H NMR (acetone-d_6) δ 6.57 (br s, 1H), 6.93 (d, $J = 8.3$ Hz, 1H), 6.98 (dd, $J = 7.3$ and 4.9 Hz, 1H), 7.47 (d, $J = 8.3$ Hz, 4H), 7.52 (td, $J = 7.8$ and 2.0 Hz, 1H), 7.55 (s, 2H), 7.57 (d, $J = 8.3$ Hz, 4H), 8.17 (dd, $J = 4.9$ and 2.0 Hz, 1H). Anal. Calcd for $C_{24}H_{15}Cl_2N_3S$: C, 64.29; H, 3.37; N, 9.37. Found: C, 64.47; H, 3.46; N, 9.30.

***N*-(2-Pyridylthio)-4-ethoxycarbonyl-2,6-bis(4-chlorophenyl)aniline (3g):** yield 69%; colorless needles; mp 172−173 °C; IR (KBr) 3330 (NH) and 1715 (CN) cm^{-1}; ^{1}H NMR (acetone-d_6) δ 1.32 (t, $J = 7.3$ Hz, 3H), 4.32 (q, $J = 7.3$ Hz, 2H), 6.46 (br s, 1H), 6.93−6.98 (m, 2H), 7.46 (d, $J = 8.3$ Hz,

(19) Ishimaru, Y.; Kitano, M.; Kumada, H.; Koga, N.; Iwamura, H. *Inorg. Chem.* **1998**, *37*, 2273.
(20) Miura, Y.; Oka, H.; Momoki, M. *Synthesis* **1995**, 1419.
(21) Miyaura, N.; Suzuki, A. *Chem. Rev.* **1995**, *95*, 2457.
(22) Kajigaeshi, S.; Kakinami, T.; Inoue, K.; Kondo, M.; Nakamura, H.; Fujikawa, M.; Okamoto, T. *Bull. Chem. Soc. Jpn.* **1988**, *61*, 597.

4H), 7.49 (t, J = 8.3 Hz, 1H), 7.54 (d, J = 8.3 Hz, 4H), 7.78 (s, 2H), 8.16 (d, J = 4.9 Hz, 1H). Anal. Calcd for $C_{26}H_{20}Cl_2N_2O_2S$: C, 63.03; H, 4.07; N, 5.65. Found: C, 62.86; H, 4.10; N, 5.44.

***N*-(2-Pyridylthio)-4-acetyl-2,6-di(phenyl-d_5)aniline (3c-d_{10}):** yield 42%; colorless prisms; mp 124−126 °C; IR (KBr) 3300 (NH), 2289 (CD), and 1660 (C=O) cm^{-1}; ^{1}H NMR (acetone-d_6) δ 2.57 (s, 3H), 6.39 (br s, 1H), 6.85 (d, J = 8.3 Hz, 1H), 6.91 (dd, J = 8.3 and 4.9 Hz, 1H), 7.45 (t, J = 8.3 Hz, 1H), 7.79 (s, 2H), 8.11 (d, J = 4.9 Hz, 1H). Anal. Calcd for $C_{25}H_{10}D_{10}N_2OS$: C, 73.85; H + D, 4.96; N, 6.89. Found: C, 73.86; H + D, 4.99; N, 6.80.

General Procedure for the Preparation of 4. To a stirred solution of an aniline (5.6 mmol) and Et_3N (3 mL) in dry ether (300 mL) was added a solution of 2-pyridinesulfenyl chloride (11.2 mmol) in CH_2Cl_2 (10 mL) dropwise at 0 °C. After completion of the addition, the mixture was stirred at 0 °C for 2 h and filtered. Filtration, evaporation, column chromatography on alumina at 0 °C (**4a**) or room temperature (**4b**−**d**) with 1:5 ethyl acetate−benzene, and crystallization from hexanes−ethyl acetate gave crystals of **4**.

***N*-(4-Pyridylthio)-2,4,6-triphenylaniline (4a):** white micropowder (not crystallized); yield 40%; IR (KBr) 3190 (NH) cm^{-1}; ^{1}H NMR (acetone-d_6) δ 6.03 (s, 1H), 6.67 (dd, J = 4.4 and 1.5 Hz, 2H), 7.31−7.36 (m, 3H), 7.44 (t, J = 7.8 Hz, 6H), 7.51 (s, 2H), 7.59 (d, J = 7.8 Hz, 4H), 7.73 (d, J = 7.8 Hz, 2H), 8.09 (dd, J = 4.4 and 1.5 Hz, 2H).

***N*-(4-Pyridylthio)-2,4,6-tris(4-chlorophenyl)aniline (4b):** colorless prisms; yield 55%; mp 198−200 °C; IR (KBr) 3324 (NH) cm^{-1}; ^{1}H NMR (acetone-d_6) δ 6.24 (s, 1H), 6.76 (dd, J = 4.4 and 1.5 Hz, 2H), 7.43 (d, J = 8.8 Hz, 4H), 7.45 (d, J = 8.8 Hz, 2H), 7.54 (s, 2H), 7.57 (d, J = 8.8 Hz, 4H), 7.77 (d, J = 8.3 Hz, 2H), 8.15 (dd, J = 4.4 and 1.5 Hz, 2H). Anal. Calcd for $C_{29}H_{19}Cl_3N_2S$: C, 65.24; H, 3.59; N, 5.25. Found: C, 65.11; H, 3.72; N, 5.10.

***N*-(4-Pyridylthio)-4-ethoxycarbonyl-2,6-bis(4-chlorophenyl)aniline (4c):** colorless needles; yield 23%; mp 165−167 °C; IR (KBr) 3142 (NH) cm^{-1}; ^{1}H NMR (acetone-d_6) δ 1.33 (t, 7.3 Hz, 3H), 4.32 (q, J = 7.3 Hz, 2H), 6.54 (s, 1H), 6.79 (dd, J = 4.4 and 1.5 Hz, 2H), 7.42 (d, J = 8.8 Hz, 4H), 7.50 (d, J = 8.8 Hz, 4H), 7.78 (s, 2H), 8.20 (dd, J = 4.4 and 1.5 Hz, 2H). Anal. Calcd for $C_{26}H_{20}Cl_2N_2O_2S$: C, 63.03; H, 4.07; N, 5.65. Found: C, 62.77; H, 3.97; N, 5.58.

***N*-(4-Pyridylthio)-2,4,6-tri(phenyl-d_5)aniline (4a-d_{15}):** colorless micropowder (not crystallized); yield 43%; IR (KBr) 3142 (NH) cm^{-1}; ^{1}H NMR (acetone-d_6) δ 6.03 (s, 1H), 6.67 (dd, J = 4.4 and 1.5 Hz, 2H), 8.09 (dd, J = 4.4 and 1.5 Hz, 2H).

General Procedure for the Isolation of Radicals. A precursor (100 mg) was dissolved in benzene (20 mL) with stirring. To the stirred solution was added K_2CO_3 (1.0 g) at once, and PbO_2 (2.0 g) was added in several portions over 2 min. After completion of the addition, the mixture continued to be stirred for an additional 0.5−1 min. After filtration, the solvent was removed by the freeze-drying method, and the resulting light green powder was crystallized from hexanes−ethyl acetate.

***N*-(2-Pyridylthio)-2,4,6-triphenylphenylaminyl (1a):** black needles; yield 40%; mp 138−140 °C. Anal. Calcd for $C_{29}H_{21}N_2S$: C, 81.09; H, 4.93; N, 6.52. Found: C, 80.97; H, 4.98; N, 6.25.

***N*-(2-Pyridylthio)-2,4,6-tris(4-chlorophenyl)phenylaminyl (1b):** green needles; yield 24%; mp 156−157 °C. Anal. Calcd for $C_{29}H_{18}Cl_3N_2S$: C, 65.36; H, 3.40; N, 5.26. Found: C, 65.22; H, 3.48; N, 5.11.

***N*-(2-Pyridylthio)-4-acetyl-2,6-diphenylphenylaminyl (1c):** purple needles; yield 33%; mp 135−136 °C. Anal. Calcd for $C_{25}H_{19}N_2OS$: C, 75.92; H, 4.84; N, 7.08. Found: C, 75.69; H, 4.85; N, 6.86.

***N*-(2-Pyridylthio)-4-acetyl-2,6-bis(4-chlorophenyl)phenylaminyl (1d):** black plates; yield 28%; mp 147−149 °C; IR (KBr) 1670 (C=O) cm^{-1}. Anal. Calcd for $C_{25}H_{17}Cl_2N_2OS$: C, 64.66; H, 3.69; N, 6.03. Found: C, 64.53; H, 3.76; N, 5.94.

TABLE 5. Crystal Data, Data Collection, Solution, and Refinement for 1a, 1c, and 1e

	1a	1c	1e
empirical formula	$C_{29}H_{21}N_2S$	$C_{25}H_{19}N_2OS$	$C_{24}H_{16}N_3S$
formula weight	429.56	359.50	378.47
crystal size/mm	0.01 × 0.01 × 0.70	0.30 × 0.10 × 0.70	0.10 × 0.20 × 0.70
crystal system	monoclinic	monoclinic	monoclinic
a/Å	19.940(2)	35.182(4)	18.805(3)
b/Å	23.668(2)	5.406(3)	13.800(2)
c/Å	9.8212(7)	10.790(8)	14.924(2)
β/deg	94.019(2)	90.59(7)	91.102(8)
V/Å^3	4623.6(6)	2052(1)	3872(1)
D(calcd)/g cm^{-3}	1.234	1.280	1.298
space group	$P2_1/a$ (No. 14)	$P2_1/a$ (No. 14)	$C2/c$ (No. 15)
Z	8	4	8
radiation	Mo Kα	Cu Kα	Mo Kα
μ/cm^{-1}	1.59	15.36	1.81
F(000)	1800.00	828.00	1576.00
temp/°C	23	23	15
no. of rflns collected	22 536	2887	7463
no. of unique rflns	10 414	2716	3897
R_{int}	0.034	0.092	0.038
rflns/params	4037/577	2020/299	1737/253
no. of rflns with $I > n\sigma(I)$	4037 (n = 1.3)	2020 (n = 1.6)	1737 (n = 0.80)
R^a	0.086	0.073	0.081
$R_w{}^b$	0.137	0.132	0.062
GOF	1.39	1.99	1.03

^{a} $R = \sum(F_o^2 - F_c^2)/\sum F_o^2$. ^{b} $R_w = [\sum w(F_o^2 - F_c^2)^2/\sum w(F_o^2)^2]^{1/2}$.

***N*-(2-Pyridylthio)-4-cyano-2,6-diphenylphenylaminyl (1e):** yield 35%; dark blue needles; mp 130−131 °C; IR (KBr) 2220 (C≡N) cm^{-1}. Anal. Calcd for $C_{24}H_{16}N_3S$: C, 76.16; H, 4.26; N, 11.10. Found: C, 76.06; H, 4.29; N, 10.88.

***N*-(2-Pyridylthio)-4-cyano-2,6-bis(4-chlorophenyl)phenylaminyl (1f):** black plates; yield 24%; mp 157−158 °C; IR (KBr) 2220 (C≡N) cm^{-1}. Anal. Calcd for $C_{24}H_{14}Cl_2N_3S$: C, 64.44; H, 3.15; N, 9.39. Found: C, 64.31; H, 3.25; N, 9.37.

***N*-(2-Pyridylthio)-4-ethoxycarbonyl-2,6-bis(4-chlorophenyl)phenylaminyl (1g):** purple needles; yield 36%; mp 117−119 °C; IR (KBr) 1705 (C=O) cm^{-1}. Anal. Calcd for $C_{26}H_{19}Cl_2N_2O_2S$: C, 63.16; H, 3.87; N, 5.67. Found: C, 63.24; H, 4.12; N, 5.38.

***N*-(4-Pyridylthio)-2,4,6-tris(4-chlorophenyl)phenylaminyl (2b):** green plates; yield 44%; mp 167−168 °C. Anal. Calcd for $C_{29}H_{18}Cl_3N_2S$: C, 65.36; H, 3.40; N, 5.26. Found: C, 65.21; H, 3.55; N, 5.14.

***N*-(4-Pyridylthio)-4-ethoxycarbonyl-2,6-bis(4-chlorophenyl)phenylaminyl (2c):** purple prisms; yield 43%; mp 141−143 °C; IR (KBr) 1715 (C=O) cm^{-1}. Anal. Calcd for $C_{26}H_{19}Cl_2N_2O_2S$: C, 63.16; H, 3.87; N, 5.67. Found: C, 62.95; H, 3.74; N, 5.67.

X-ray Crystallographic Analysis of 1a. A black needle crystal was mounted on a glass fiber. All measurements were made on a Rigaku RAXIS-RAPID Imaging Plate diffractometer with graphite-monochromated Mo Kα radiation (λ = 0.710 69 Å). The data were collected to a maximum 2θ value of 55.0°. A total of 44 images, corresponding to 220.0° oscillation angles, were collected with two different goniometer settings. The exposure time was 2.50 min/deg. The camera radius was 127.40 mm. Readout was performed in the 0.100-mm pixel mode. Data were processed by the PROCESS-AUTO program package.

The structure was solved by direct methods (SIR92)[23] and expanded using Fourier techniques. The non-hydrogen atoms were refined anisotropically. Hydrogen atoms were placed in the fixed position and not refined.[24] Crystal data and details of the data collection are summarized in Table 5.

(23) Altomare, A.; Burla, M. C.; Camalli, M.; Cascarano, M.; Giacovazzo, C.; Guagliardi, A.; Polidori, G. *J. Appl. Crystallogr.* **1994**, *27*, 435.

X-ray Crystallographic Analysis of 1c. A dark green plate crystal was mounted on a glass fiber. All measurements were made on a Rigaku AFC7R diffractometer with graphite-monochromated Cu Kα radiation (λ = 1.541 78 Å). The data were collected using the $\omega - 2\theta$ scan technique to a maximum 2θ value of 113.5°. The linear absorption coefficient, μ, for Cu Kα radiation is 15.4 cm^{-1}. Azimuthal scans of several reflections indicated no need for an absorption correction.

The structure was solved by direct methods (SHELXS86)[25] and expanded using Fourier techniques. The non-hydrogen atoms were refined anisotropically, and all hydrogen atoms were placed at the calculated positions and not refined.[24] One of the phenyl rings is disordered over two sites with an occupancy of 0.5 and 0.5 [C(20, 21, 22, 23, 24, 25) and C(20, 26, 27, 23, 28, 29)]. Crystal data and details of the data collection are provided in Table 5.

X-ray Crystallographic Analysis of 1e. A black needle crystal was mounted on a glass fiber. All measurements were made on a Rigaku RAXIS-RAPID Imaging Plate diffractometer with graphite-monochromated Mo Kα radiation (λ = 0.710 69 Å). The data were collected to a maximum 2θ value of 55.0°. A total of 44 images, corresponding to 220.0° oscillation angles, were collected with two different goniometer settings. Exposure time was 2.50 min/deg. The camera radius was 127.40 mm. Readout was performed in the 0.100-mm pixel mode. Data were processed by the PROCESS-AUTO program package.

The structure was solved by direct methods (SIR92)[23] and expanded using Fourier techniques. The non-hydrogen atoms were refined anisotropically. Hydrogen atoms were placed in the fixed position and not refined.[24] Crystal data and details of the data collection are provided in Table 5.

Acknowledgment. This work was in part supported by a Grant-in-Aid for Scientific Research on Priority Area (A; No. 10146246) from the Ministry of Education, Science, Sports and Culture, Japan.

Supporting Information Available: X-ray crystallographic data for **1a**, **1c**, and **1e**. This material is available free of charge via the Internet at http://pubs.acs.org.

JO0205659

(24) All calculations were performed using the teXsan crystallographic software package of the Molecular Structure Corporation.

(25) Sheldrick, G. M. *Crystallographic Computing 3*; Sheldrick, G. M., Kruger, C., Goddard, R., Eds.; Oxford University Press: London, 1985; pp 175−189.